Fouling behavior of protein in mixed solvent systems: A combined experimental and simulation study

Journal of Membrane Science 693 (2024) 122361

Contents lists available at ScienceDirect

Journal of Membrane Science

journal homepage: www.elsevier.com/locate/memsci

Fouling behavior of protein in mixed solvent systems: A combined experimental and simulation study

Angie Qi Qi Ng [a,b,c,1], Yunqiao Ma [a,b,c,1], Henry J. Tanudjaja [a,f], Navin Raj Tamilselvam [a], Rong Wang [b,d], Jia Wei Chew [a,b,e,*]

[a] School of Chemical and Biomedical Engineering, Nanyang Technological University, Singapore, 637459, Singapore
[b] Singapore Membrane Technology Centre, Nanyang Environment and Water Research Institute, Nanyang Technological University, Singapore, 637141, Singapore
[c] Interdisciplinary Graduate Programme, Graduate College, Nanyang Technological University, Singapore, 637335, Singapore
[d] School of Civil and Environmental Engineering, Nanyang Technological University, Singapore, 639798, Singapore
[e] Chemical Engineering, Chalmers University of Technology, 412 96, Gothenburg, Sweden
[f] Environmental Science and Engineering, Division of Biological and Environmental Science and Engineering (BESE), King Abdullah University of Science and Technology (KAUST), Thuwal, 23955-6900, Kingdom of Saudi Arabia

ARTICLE INFO

Keywords:
Molecular dynamics simulation
Free energy of adsorption
Membrane fouling
Organic solvent mixture
Solvation film

ABSTRACT

Membrane fouling in organic solvent environments remains poorly explored despite its significance in chemical and pharmaceutical industries. This study uses molecular dynamics (MD) simulations and experiments to explore lysozyme fouling in water, as well as four organic solvent environments, namely, 30 % v/v and 50 % v/v isopropyl alcohol (IPA), and 30 % v/v and 50 % v/v dimethyl sulfoxide (DMSO). Experimentally, flux declines were least with IPA and worst with DMSO. Biased simulations indicate the worst fouling in DMSO is tied to the most attractive lysozyme-membrane energy in the presence of DMSO. However, the relative attractive energies for IPA and water do not agree with the relative flux declines, indicating other factors are more influential when the interaction energies are similar. To understand the gentler flux decline for IPA despite the more attractive lysozyme-membrane energy, radial distribution functions (RDFs) were obtained from unbiased simulations. Analyss of the water and solvent films around both the membrane and the lysozyme molecule reveal that the denser water film around both entities induced by the presence of IPA serves as a barrier for fouling and thus leads to less flux decline. The results underscore the complexity of fouling in organic solvent systems, cautioning against direct use of the understanding based on aqueous systems.

1. Introduction

Membrane technology has emerged as a promising and versatile solution for various separation processes across many industries spanning food processing, biotechnology, and pharmaceuticals [1–3]. However, one of the challenges with membrane technology is membrane fouling, whereby the deposition of materials on the membrane results in a reduction of flux [4]. This phenomenon unfortunately leads to a lowering of the effectiveness and efficiency of the separation process over time [5]. To mitigate membrane fouling, a deeper understanding of the membrane fouling mechanism is required to guide new strategies to improve the membrane filtration operation in practice. Despite much knowledge accumulated concerning membrane fouling in water, the corresponding understanding in organic solvents, or a mixed system involving organic solvents, which is commonly utilized in industries, remains rather limited [6,7]. Many industrial operations are carried out in organic solvent environment due to advantages like increased solubility, stability, and reaction kinetics. The reported studies on membrane fouling in water systems have been found to fall short of describing membrane fouling for the organic solvents commonly used in industries. Liu et al. reviewed the recent research related to the preparation of hollow fiber (HF) organic solvent nanofiltration membranes, and found that the separation mechanisms in aqueous systems cannot be directly applied to organic solvent systems due to the different physical properties, such as the charge effect in aqueous systems that is negligible in organic solvent systems [8]. Lay and Chew analyzed the critical flux of

* Corresponding author. School of Chemical and Biomedical Engineering, Nanyang Technological University, Singapore, 637459, Singapore.
E-mail address: jia.chew@chalmers.se (J.W. Chew).
[1] These authors contributed equally to this work.

https://doi.org/10.1016/j.memsci.2023.122361
Received 5 October 2023; Received in revised form 6 December 2023; Accepted 16 December 2023
Available online 23 December 2023

silica particles in cross-flow ultrafiltration, and reported that the shear-induced diffusion model did not apply for ethanol and hexane, but did for water and formamide [9]. Clearly, while much knowhow has been advanced on membrane fouling in water environments, numerous gaps with respect to membrane fouling in organic solvent-based membrane-filtration processes exist.

Past studies have advanced our understanding of membrane fouling in organic solvents, including correlating interfacial interactions with membrane fouling [10–12], quantifying critical flux [9], elucidating fouling mechanisms using fouling models [13,14], demonstrating different flux behaviors [15–17], and modifying membranes to mitigate fouling [18]. However, such experimental and modeling methods fall short of providing the molecular-scale insights underlying some observations [19,20]. To this end, molecular dynamics (MD) simulation is a useful tool based on atomistic force field parameters and solves Newton's equations of motions to capture various phenomena on the nanometer scale (e.g., intermolecular interactions, molecular trajectory). While DLVO or XDLVO models can provide for interfacial interaction energy, MD simulations can additionally give useful information related to membrane fouling like foulant trajectories, foulant-membrane distance, and density and proximity of solvation shells. Particularly for macromolecular foulants like proteins, whereby the charges are non-uniform, the constituent amino acid residues have been shown to dictate fouling [21,22], suggesting the inadequacy of DLVO-type models and thus the importance of MD simulations to bridge the gap. Also, while MD simulations cannot model the various fouling mechanisms (e.g., pore blocking, pore constriction) due to the limited spatial-scale, they reveal the molecular-level behaviors underlying the fouling phenomena. Furthermore, while MD simulations fall short in providing direct information on fouling reversibility or irreversibility, inference can be made through the foulant-membrane interaction energy. Nonetheless, through revealing free energy profiles, radial distribution functions, foulant mobility, etc., MD simulations offer valuable insights into membrane fouling propensity for different foulants and membranes in different solvents [20]. Therefore, MD as a computational technique has become increasingly popular to complement experimental results to obtain more understanding about membrane fouling [19,20,23–25]. Mollahosseini et al. performed MD simulations with only one protein structure, and assessed the bonding affinity of the protein within the protein-ceramic membrane model by quantifying the number of bonds between water as well as the solvated protein with the membrane surface [26]. Ma et al. highlighted the importance of local interactions in governing protein fouling behavior, which explains why macroscopic measurements like zeta potential of foulant and membrane are known to fall short of predicting membrane fouling extents [21,22]. Additionally, it was shown via MD simulations that, other than the well-reported foulant-membrane interactions, the competitive adsorption between solvent and foulant onto the membrane has a significant effect on the extent of fouling [27]. Regarding membrane fouling by macromolecules in mixed-solvents environments, MD simulations are expected to provide valuable insights on the multifaceted phenomena. This motivated the current study.

Lysozyme was studied here, since it is a relatively small protein with stable and well-known folding patterns, which allows investigation under different experimental conditions without significant degradation [28]. Also, since the structure of lysozyme has been extensively studied [29], it serves as a well-characterized model system to investigate the mechanisms of macromolecular fouling, which can then be a valuable benchmark for other macromolecular foulants with non-uniform charges. Since different solvent environments have been known to affect the fouling behavior, this study focused on lysozyme fouling in two different concentrations of isopropyl alcohol (IPA) in water and two different concentrations of dimethyl sulfoxide (DMSO) in water. DMSO and IPA were selected as the solvents due to their frequent use in the pharmaceutical industry, especially in chemical reactions as well as purification processes [30–33]. As organic solvent filtration applications proliferate, the results here contribute to the knowledge base by benchmarking the effect of different organic solvents against that of the well-studied water systems.

Accordingly, this study used a dead-end filtration cell to evaluate fouling of aluminum oxide membranes by lysozyme during ultrafiltration in five different solvent environments at the same transmembrane pressure (TMP). The concentrations of IPA or DMSO tested were up to 50 % v/v of solvent in water, which is the highest limit for dissolving lysozyme particularly for DMSO [34,35]. Specifically, five solvent systems assessed were water, 30 % v/v IPA in water, 50 % v/v IPA in water, 30 % v/v DMSO in water and 50 % v/v DMSO in water. In parallel, MD simulations were carried out to provide molecular-level insights on fouling to supplement the experimental results by quantifying the free energy terms and generating dynamic trajectories of the lysozyme molecule. Steered molecular dynamics (SMD) simulations (or biased MD simulations) were conducted to compute the free energy profile of lysozyme and the membrane in the different solvents. In addition, unbiased simulations were performed to assess the adsorption frequency of lysozyme, followed by generating the radial distribution function (RDF) plots. The coupling of experimental and simulation results is expected to provide insightful mechanistic understanding into fouling behaviors in various solvent environments.

2. Methodology

2.1. Materials

Whatman Anopore aluminum oxide membranes, which are resistant to organic solvents, were used in this study. Each Anodisc membrane, which had nominal pore sizes of 0.1 μm and was 47 mm in diameter, had straight-through pores and narrow pore size distributions.

The foulant employed in the experiment was lysozyme (Sigma-Aldrich, product number A7906), with a molecular weight of approximately 66 kDa. Lysozyme is well characterized [36,37] and served here as a model protein to understand protein fouling.

The solvents used included deionized (DI) Water obtained from the Milli-Q DI Water Purification System (Merck-Millipore; Massachusetts, USA), dimethyl sulfoxide (DMSO; Fisher Scientific; analytical reagent grade >99.9 %), and isopropyl alcohol (IPA, Aik Moh Singapore). For the MD simulation, the chemical structures of DMSO and IPA are drawn using Discovery Studio, as presented in Figure A2 and Table A1. Water, IPA and DMSO are all polar; however, DMSO is polar aprotic (i.e., cannot form hydrogen bond), while water and IPA are polar protic (i.e., can form hydrogen bond) solvents.

2.2. Experimental setup and protocol

The dead-end constant-pressure ultrafiltration setup is illustrated in Fig. 1a. All parts in contact with IPA and DMSO had to be stainless steel or polytetrafluoroethylene (PTFE) for chemical resistance to the solvents. The membrane-filtration cell was custom-made with a stainless steel cylinder (8 mm inner diameter and 14.8 cm height) atop supports that house the membrane (details in Fig. 1b), and had an active membrane area of 1 cm^2. A compressed air cylinder (Leeden) provided the pressure needed to drive the filtration, the feed tank sat on a magnetic stirrer device (MR Hei-Tec; Heidolph) to ensure uniform dispersion of the feed, a PTFE diaphragm pressure gauge (Sigma Aldrich) maintained the transmembrane pressure (TMP), the permeate tank sat on a weighing balance (Mettler-Toledo; ML4002) to measure the change in permeate mass, while a computer logged the data at 60 s interval via the Balance Link software and calculated the flux using MATLAB 2019A. The permeate flux (J) was calculated by permeate volume collected (V) divided by the product of membrane active area (A) and time interval between two recorded permeate volume data (i.e., 60 s):

$$J = \frac{V}{A \times t} \quad \text{Eq. (1)}$$

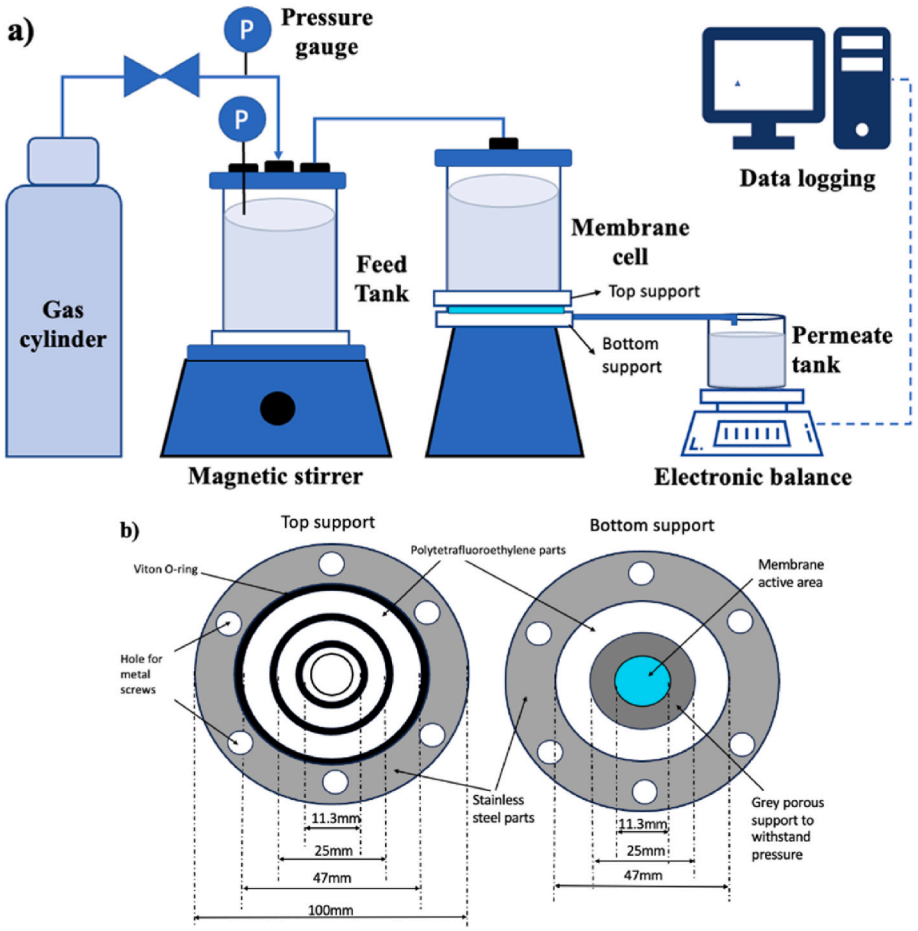

Fig. 1. Schematic diagrams of (a) dead-end filtration setup, and (b) details of membrane cell.

Five different solvent environments were assessed, namely DI water, 30 % v/v of IPA in DI water, 50 % v/v of IPA in water, 30 % v/v of DMSO in DI water, and 50 % v/v of DMSO in water. It should be noted that the upper limit was set at 50 %, because of the tendency of lysozyme to denature and aggregate at higher concentrations [34,35]. Prior to each test, 400 mL of the targeted feed was prepared, and 200 mg of lysozyme was added, giving a lysozyme concentration of 0.5 g/L. Given that lysozyme readily dissolves in DI water, for each of the four organic solvent mixtures, 200 mg of lysozyme was first dissolved in DI water and stirred for 5 min, then the organic solvent was added and stirring continued for an additional 15 min. To ensure uniform dispersion, each feed was stirred by a magnetic stirrer bar at 500 rpm for a total of 20 min before each experiment.

During each filtration test, the feed was continuously stirred at 500 rpm. The TMP value was set at 2 bar throughout each experiment that lasted 100 min. Each condition was tested three times to check for reproducibility and a fresh membrane was used for each test.

2.3. MD simulations

The molecular structures of foulant, membrane, and solvent were first built separately. The lysozyme molecule was directly downloaded from the Protein Data Bank (ID: 253L), which has been used in earlier membrane fouling studies [21,22]. CHARMM-GUI [38] was used to protonate amino acid residues in lysozyme, which results in an overall charge of +9e at neutral pH. The Anopore inorganic membrane made from Al_2O_3 had been modeled in an earlier study [39], so the same three dimensional crystal structure and force field parameters were used in this study [40]. Topology files of all solvent molecules were directly generated from CHARMM-GUI. CHARMM36 m force field parameters were assigned to lysozyme and solvent molecules [41], with 2D dihedral correction map (CMAP) incorporated for the lysozyme backbone to improve computational accuracy [42].

After obtaining individual structure files, CHARMM-GUI facilitated a convenient system packing of all species, with representative images shown in Fig. 1. The dimensions of the simulation box were about 100 Å× 100 Å × 110 Å, with the alumina membrane fixed at the bottom throughout the simulation to avoid drifting. Lysozyme was then placed in the center of the box with six different initial orientations to capture possible adsorption onto the membrane surface, as per a previous study that found local interactions were dominant [22]. Hence, for each solvent, six replicate MD runs were made. Finally, the rest of the simulation box was filled randomly with the corresponding solvent molecules.

2.4. Unbiased simulation and SMD

After assigning force field parameters to all species and packing the system into the desired geometry shown in Fig. 2, the MD simulations were conducted in the Large-scale Atomic/Molecular Massively Parallel Simulator (LAMMPS) [43]. To boost the simulation efficiency, the SHAKE algorithm [44] was applied to constrain all covalent bonds containing hydrogen atoms to be rigid. A cut-off distance of 12 Å was used for non-bonded Lennard-Jones interaction, which is a commonly chosen value in MD studies related to membrane filtration [45,46]. Periodic boundary condition was applied in all three directions. The Particle-Particle Particle-Mesh (PPPM) method was employed for the calculation of long-ranged electrostatic interaction in the reciprocal space. Visual Molecular Dynamics (VMD) [47] was used for

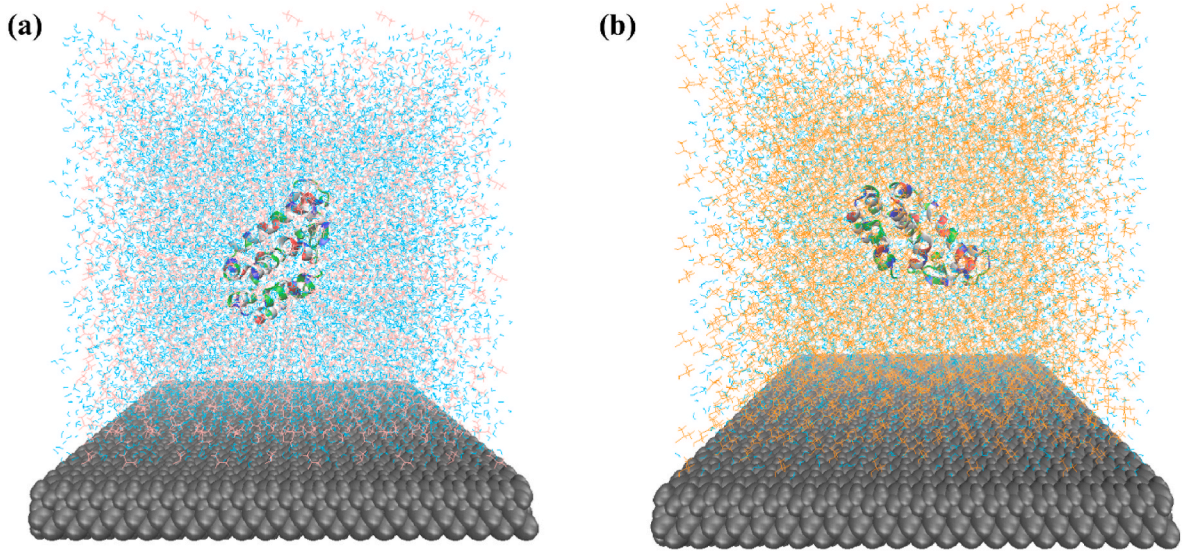

Fig. 2. Representative schematics of the initial MD system, with solvent composition of (a) 30 % v/v DMSO; and (b) 50 % v/v IPA. Alumina membrane is shown as the grey slab at the bottom of the simulation box, drawn with VDW style in VMD. Lysozyme (with two different initial orientations in the two subplots) is drawn with NewCartoon style and colored according to the amino acid residue nature: white for non-polar, blue for basic, red for acidic, and green for polar. Solvent molecules are depicted by Line style, with cyan color for water, pink color for DMSO, and orange color for IPA. (For interpretation of the references to color in this figure legend, the reader is referred to the Web version of this article.)

post-processing of the simulation trajectories.

Before using the enhanced sampling algorithm to calculate the potential mean force (PMF) profile of lysozyme, systems must be equilibrated and run in an unbiased manner first (i.e., no external force added to lysozyme) to ensure convergence of free energy calculation [48]. With a time step of 2 fs, unbiased simulations were conducted for each system for 100 ns under canonical ensemble (NVT) with temperature fixed at 298 K using a Nosé-Hoover thermostat [49].

Biased simulations were conducted for each system subsequently to quantify the PMF profile of lysozyme with respect to the alumina membrane surface. One of the key benefits of biased simulation is to force systems to visit all states of interest, since some of them may not be readily accessible in unbiased simulation due to high energy barriers [50]. To achieve that, external bias is added to the system such that the free energy profile can be recovered by properly accounting for the influence of external force [51]. The reaction coordinate ξ of biased simulation, which is the 1D coordinate through which the system progresses, is defined to be the difference in z-coordinate between the center-of-mass (COM) of lysozyme and surface hydrogen atoms of alumina membrane. In other words, free energy was computed as a function of the lysozyme-membrane separation distance via enhanced sampling algorithm. Here we chose to apply SMD, which is a nonequilibrium approach with relatively smaller computational cost [52,53], and has been extensively used in past studies to explore the adsorption of proteins to various surfaces [54–56]. Essentially, a harmonic potential $w(\mathbf{r};\ \lambda_t)$ is applied to the adsorbed adsorbate (lysozyme in this case), and gradually pull it away from the surface:

$$w(\mathbf{r};\ \lambda_t) = \frac{K}{2}[\xi(\mathbf{r}) - \lambda_t]^2 \qquad \text{Eq. (2)}$$

$$\lambda_t = \lambda_0 + vt \qquad \text{Eq. (3)}$$

where $\mathbf{r}$ is the positional vector of atoms in the system, λ_t is the center of the applied harmonic potential at time t which moves with a velocity of v, K is the force constant which should be large enough to let the stiff-spring approximation remain valid [57]. In this study, K was chosen to be 100 $\frac{kcal}{mol \bullet \text{Å}^2}$, with a pulling velocity of 5 $\frac{\text{Å}}{ns}$, so that reaction coordinate ξ closely follows the evolution of λ. It should be noted that the dynamic pulling of lysozyme started at the configuration whereby lysozyme was adsorbed to the membrane surface, and stopped when lysozyme was fully detached and entered the bulk liquid region, which is evidenced by the plateau of the free energy ΔF. For each solvent composition, there were 18 pulling processes performed, with starting configurations corresponding to time points of 50 ns, 70 ns, and 100 ns of each of the six independent runs. If lysozyme was found to be unadsorbed at any time point, as suggested by Meißner et al. [58], lysozyme was first pushed toward the membrane surface with an external force and subsequently equilibrated by removing the added force, followed by the normal SMD pulling process. In each SMD pulling process, the amount of external work done W was recorded every 10,000 time steps:

$$W = -Kv\int_0^t \left[\xi\left(\mathbf{r}|_{t'}\right) - \lambda_0 - vt'\right]dt' \qquad \text{Eq. (4)}$$

Free energy ΔF was computed via the Jarzynski's equality:

$$e^{-\beta\Delta F} = \langle e^{-\beta W}\rangle \qquad \text{Eq. (5)}$$

where β is the inverse temperature ($1/k_BT$), and the operator means the ensemble average of all pulling trajectories. The reference zero-point for free energy was selected to be the maximum value of ξ.

3. Results and discussion

3.1. Flux decline

Fig. 3 shows the normalized flux decline trends with respect to time for 0.5 g/L of lysozyme in various solvent environments up to 30 min. Specifically, for fair comparison among the feeds in view of the dissimilar initial fluxes, each flux value was normalized with respect to the initial flux. The TMP was set to 2 bar and each experiment lasted 100 min, beyond which there was negligible change in flux decline. Fig. 3 shows typical trends for protein filtration, specifically in that the initial flux decline is steep due to concentration polarization, and subsequently gentler as proteins progressively deposit onto the membrane [7,59,60]. Each error bar represents the span of the data obtained from triplicates of each feed. The error bars are the largest for 50 % v/v DMSO, reflecting the greater variability for this system, though the underlying reason is not clear. The different rates of flux decline for the same lysozyme

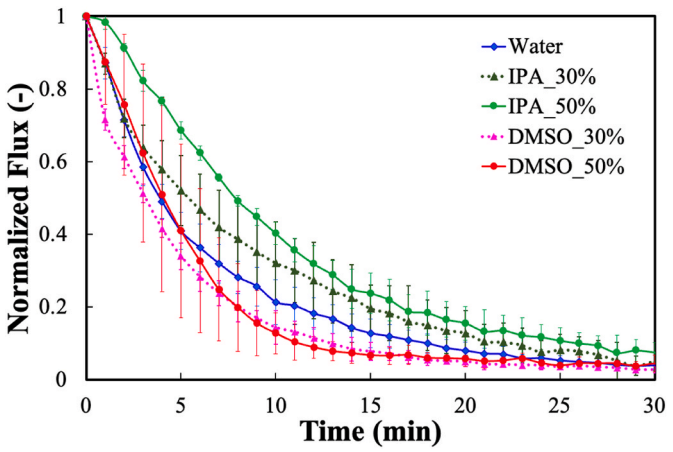

Fig. 3. Trends of normalized flux with respect to time for filtration experiments of 0.5 g/L lysozyme in different solvent systems operated at a constant TMP of 2 bar. Each error bar represents the span of the data obtained from triplicates of each feed.

foulant indicate that the solvent significantly affected the fouling phenomena, which agrees with earlier studies [10,13,61]. In particular, DMSO gave worse flux declines than IPA, which indicates worse fouling rates in the former. Some studies compare flux declines at the same permeate volume instead of time, and thus Fig. A1a presents the flux decline trends with respect to permeate volume, indicating that water gave the least flux decline, followed by IPA and then DMSO. Consistent with Fig. 3, DMSO caused worse flux decline than IPA. However, the gentlest water decline in Fig. A1a seem to contradict that in Fig. 3, which is tied to the initial water flux (average of 28.1 mL/cm^2/s) being two-to three-fold that for the cases with IPA (averaging 8.1–12.5 mL/cm^2/s) or DMSO (averaging 11.3–17.1 mL/cm^2/s). To correct for the distinctly different permeation rates, Fig. A1b normalizes the permeate volume (i.e., cumulative permeate volume normalized with respect to the total permeate volume), making the relative trends similar to that in Fig. 3.

3.2. Free energy of interfacial interaction

Fig. 4 presents the potential mean force (PMF) curves of lysozyme with respect to the membrane surface in water, 50 % v/v IPA and 50 % v/v DMSO, which are generated using steered molecular dynamics (SMD) simulations. The PMF curve cannot be determined accurately in unbiased simulations as the system configurations or orientations are not sufficiently sampled within the limited time scale [57,62]. In other words, unbiased simulations cannot explore multiple position states or ranges, and thus fall short for generating a representative PMF curve [48,57,63]. Here, the free energy profile was generated by performing SMD, a form of biased simulation, so that external forces can be applied to the lysozyme molecules and simulate their movement to overcome the high energy barriers with the membrane surface in various solvent systems [64]. The ΔF values monotonically increase with respect to reaction coordinate ξ for lysozyme in all three solvent environments. This implies it is energetically favorable for lysozyme to approach the membrane surface from the bulk liquid in all cases.

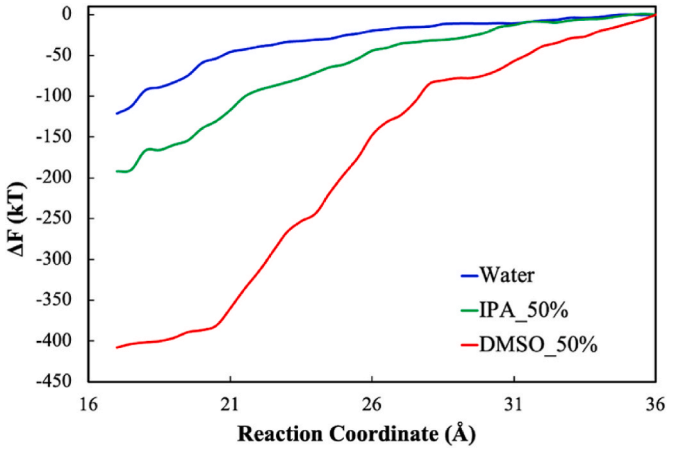

Fig. 4. PMF curves of lysozyme with respect to the membrane surface in water, 50 % v/v IPA and 50 % v/v DMSO. Free energy values are computed based on ensemble average of all SMD pulling runs in each solvent composition (Eq. (5)). Curves are shifted so that free energy values at the maximum reaction coordinate of 36 Å are zero.

The relationship between the PMF and flux decline profiles is worth highlighting. Firstly, the most negative ΔF is in 50 % v/v DMSO, whose absolute value is approximately four times that in water and twice that in 50 % v/v IPA system. This implies that lysozyme is most strongly attracted to the membrane surface in 50 % v/v DMSO, which agrees with the worst flux decline (Fig. 3). Secondly, although the free energy of absorption is more attractive in 50 % v/v IPA than in water, the flux decline was gentler in the former (Fig. 3). This suggests that, when the ΔF values are more similar, other influences may play more important roles in governing the fouling behavior. This is congruent with a recent review that indicated that the extent of fouling is dependent on various types of instantaneous interactions happening concurrently within the system rather than a single interaction energy term [20].

Hence, the biased simulation results provide the explanation that the most extensive fouling in DMSO is due to the very significant lysozyme-membrane interaction, but falls short for explaining the relative difference between IPA and water due to the more similar ΔF values between the two. To address the differences in fouling behavior in IPA versus water, unbiased simulation results are discussed as follows.

3.3. Minimum distances between lysozyme and membrane

The differences in the flux decline behaviors of the five solvent environments (Fig. 3) are further elucidated with the scatter plot in Fig. 5, which summarizes the minimum distances between lysozyme and membrane (d_{min}) for different solvent systems measured at different time points during the simulation (namely, 50 ns, 70 ns and 100 ns). Fig. 5 is generated using unbiased simulations (i.e., no external force added). The calculation method used is the same as our previous study

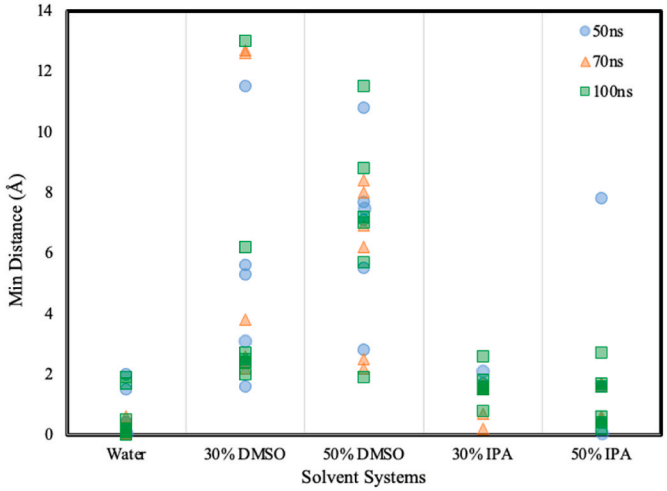

Fig. 5. Scatter plot of the distribution of d_{min} sampled from three time points (50 ns, 70 ns and 100 ns) of all 30 unbiased simulation runs in different solvent systems. Identical markers falling into the same column represent duplicate runs starting from different initial orientation of lysozyme.

[22]. For each solvent system, the unbiased simulations were run six times for different initial orientations of the lysozyme foulant, resulting in a total of 30 unbiased simulations run for the five solvent systems.

To determine the affinity of lysozyme with respect to the membrane, one way is to evaluate the distance of the lysozyme molecule from the membrane surface. A small d_{min} value means that the lysozyme stays closer to the membrane, which implies a greater lysozyme-membrane affinity and thus a higher fouling tendency. Throughout the 100 ns, Fig. 5 shows that lysozyme exhibits a large range of d_{min} values in DMSO, while small d_{min} values in water and IPA. Two highlights are noted. Firstly, the widest scatter of d_{min} values in the presence of DMSO implies the lysozyme-membrane affinity is highly dependent on the initial lysozyme orientation and time step at which the distance is measured at. This suggests that, even though the free energy of lysozyme-membrane attraction is the greatest in the presence of DMSO (Fig. 4), it is not directly related to the lysozyme-membrane distance. In other words, the significantly greater lysozyme-membrane attraction in DMSO (Fig. 4) governs the steepest flux decline (Fig. 3) rather than d_{min}. Secondly, d_{min} is inadequate to differentiate the fouling behavior in water versus IPA.

Fig. 5 implies other factors are at play rather than distance per se. It should be noted that the inadequacy of such an unbiased MD setup could be due to the insufficient spatial and time scales, which cautions the use of such models for predictive purposes. Accordingly, the radial distribution functions (RDF) among the solvent, lysozyme and membrane are evaluated to further probe the effect of the different solvents on lysozyme fouling.

3.4. Solvent films

The hydration and solvation films formed in different solvent environments were investigated using the RDF plots between solvent molecules and membrane, water molecules and lysozyme, as well as organic solvent molecules and lysozyme. The RDF plots, which were generated via unbiased simulation, are used to describe the spatial distribution or local clustering behavior of one type of molecule around another of interest. It is denoted by *g*, representing the probability of finding a pair of selected atoms at a specific distance *r* relative to the average probability value [65]. The RDF is represented in Equation (6), where *V* represents volume of the system and *p(r)* is the number of atom pairs within the spherical shell from distance *r* to $r + \Delta r$.

$$g(r) = \frac{Vp(r)}{4N\pi r^2 \Delta r} \quad \text{Eq. (6)}$$

The RDF plot is commonly used to illustrate the distribution of solvent molecules around the foulant or membrane, which can be regarded as a representation of the solvation film layer formed around the foulant or membrane. This can be related to the solvation/desolvation or hydrogen-bond forming tendencies [27,66,67].

3.4.1. Hydration and solvation films on the membrane

The aluminum oxide surface naturally has hydroxyl groups (-OH) formed after exposure to air or water. When creating the aluminum oxide membrane for molecular dynamics simulations, these hydrogen atoms attached to the membrane are included to accurately depict the interactions between the membrane surface and solvent molecules. Fig. 6 shows the RDF plots between the hydrogen atoms on the membrane surface, and either the oxygen atoms of the solvent (Fig. 6a) or of water (Fig. 6b). A taller peak indicates a denser solvent film, while a peak at a smaller r value reflects a more tightly bound film. Between Fig. 6a and b, the peak values are higher for the latter, reflecting denser water films than that formed by IPA or DMSO. Notably, Fig. 6b indicates that the water films on the membrane are thickened in the presence of IPA or DMSO, which poses a barrier to the adhesion of lysozyme onto the membrane. An earlier experimental study has also shown that denser solvation films are tied to less fouling [27]. While the thicker water film induced by DMSO is overshadowed by the marked lysozyme-membrane attraction (Fig. 5), that induced by IPA plays a role in deterring lysozyme adhesion onto the membrane and thus results in a gentler flux decline relative to that in water alone. In particular, the significantly denser water film in the case of 50 % v/v IPA correlates well the gentlest flux decline (Fig. 3).

3.4.2. Hydration and solvation films on lysozyme

To understand the nature of the hydration films around lysozyme, Fig. 7 presents the RDF analysis between the oxygen of the water molecule with respect to the nitrogen and oxygen atoms in the amino side chains of lysozyme. The representation by two different atoms provides more confidence to the RDF profiles. In both Fig. 7a and b, while the water films are consistently at the same positions, the water films are thicker in the presence of IPA or DMSO. As with Fig. 6b, in the presence of IPA, the denser water films around lysozyme deter the adherence of the lysozyme onto the membrane, leading to a gentler flux decline relative to that in water alone (Fig. 3).

On top of the water films formed around lysozyme in Fig. 7, the corresponding organic solvent films are also assessed in Fig. 8. Similar to Fig. 7, two representative atoms on the side chain of lysozyme were evaluated. Focusing only on IPA versus water, Fig. 8a shows similar peak magnitudes, while Fig. 8b shows the water film being about twice as dense as that of IPA. Nonetheless, the highest water peak value of approximately 2 (Fig. 8b) pales in comparison to the density of the water films formed in the presence of IPA (Fig. 7a and b). Therefore, the denser water films formed around lysozyme in the presence of IPA underlies the gentler flux declines relative to that in water alone (Fig. 3).

4. Conclusion

This study was conducted to understand membrane fouling by lysozyme in organic solvent - aqueous mixtures (namely, 30 % v/v IPA, 50 % v/v IPA, 30 % v/v DMSO and 50 % v/v DMSO), benchmarked

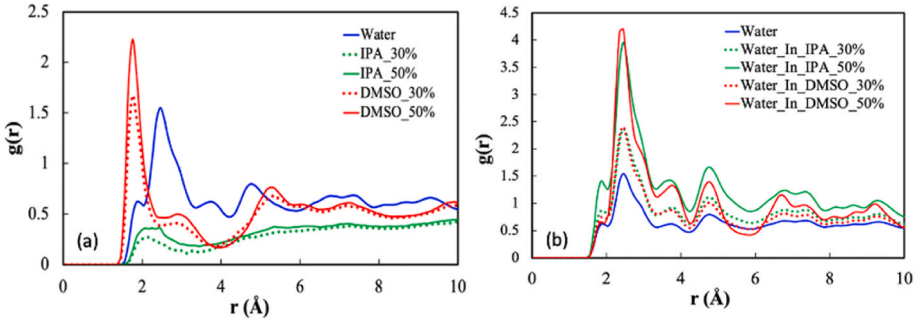

Fig. 6. Solvation/hydration of membrane: RDF between the hydrogen atoms on alumina membrane surface and oxygen atoms of (a) solvent molecules; and (b) water molecules.

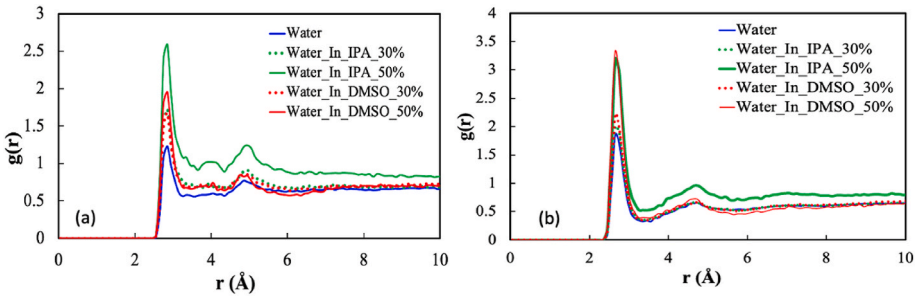

Fig. 7. Hydration of lysozyme: RDF between the oxygen atoms in water molecules and two different atoms in the amino acid side chains to represent the lysozyme: (a) selected atoms in amino acid side chains are nitrogen atoms; and (b) selected atoms in amino acid side chains are oxygen atoms.

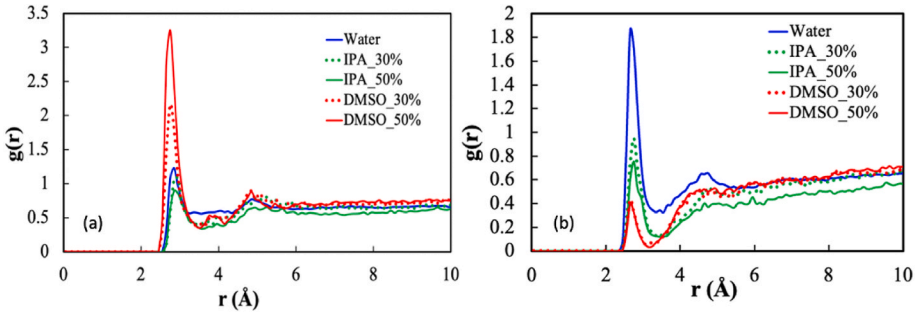

Fig. 8. Solvation of lysozyme: RDF between the oxygen atom of the solvent molecules and two different atoms in the amino acid side chains to represent the lysozyme: (a) selected atoms in amino acid side chains are nitrogen atoms; and (b) selected atoms in amino acid side chains are oxygen atoms.

against the DI water environment. Dead-end filtration of lysozyme was performed under the different solvent environments to determine the flux decline profiles, and both biased and unbiased molecular dynamics (MD) simulations were performed in parallel to provide molecular-scale insights. It should be noted that MD simulations are particularly crucial for macromolecular foulants like proteins with non-uniform charges, because membrane fouling extents have been reported to be poorly correlated with macroscopic characterizations due to the governance by local interactions.

Results indicate that the presence of organic solvent changes the fouling behavior by lysozyme. The flux decline profiles show that the presence of DMSO led to the worst fouling, followed by water and finally IPA. Biased simulations reveal that the worst flux decline in the presence of DMSO is primarily due to the significantly greater lysozyme-membrane free energy of adsorption. However, because the more similar ΔF values between water and 50 % v/v IPA are inadequate to explain the gentlest flux decline for the latter, the RDF plots generated via unbiased simulations were assessed to understand the roles of the hydration and solvation films formed around the membrane and lysozyme. The gentlest flux decline in 50 % v/v IPA is tied to the densest water film induced, which serves as a barrier to lysozyme adsorption and thus mitigates fouling.

The results here thereby demonstrate that the presence of organic solvent interferes with the interactions between the foulant and the membrane, with the dominant mechanism that governs flux decline being different depending on the solvent.

CRediT authorship contribution statement

Angie Qi Qi Ng: Formal analysis, Methodology, Writing – original draft, Writing – review & editing. **Yunqiao Ma:** Conceptualization, Formal analysis, Investigation, Methodology, Writing – original draft. **Henry J. Tanudjaja:** Formal analysis, Investigation, Methodology, Writing – original draft. **Navin Raj Tamilselvam:** Investigation. **Rong Wang:** Project administration, Supervision. **Jia Wei Chew:** Conceptualization, Formal analysis, Investigation, Methodology, Project administration, Resources, Supervision, Writing – original draft, Writing – review & editing.

Declaration of competing interest

The authors declare that they have no known competing financial interests or personal relationships that could have appeared to influence the work reported in this paper.

Data availability

Data will be made available on request.

Acknowledgement

This study was supported by A*STAR (Singapore) Advanced Manufacturing and Engineering (AME) under its Pharma Innovation Programme Singapore (PIPS) (A20B3a0070); A*STAR (Singapore) Advanced Manufacturing and Engineering (AME) under its Individual Research Grant (IRG) program (A2083c0049); and the Singapore Ministry of Education Academic Research Tier 1 Grant (2019-T1-002-065; RG100/19).

Appendix

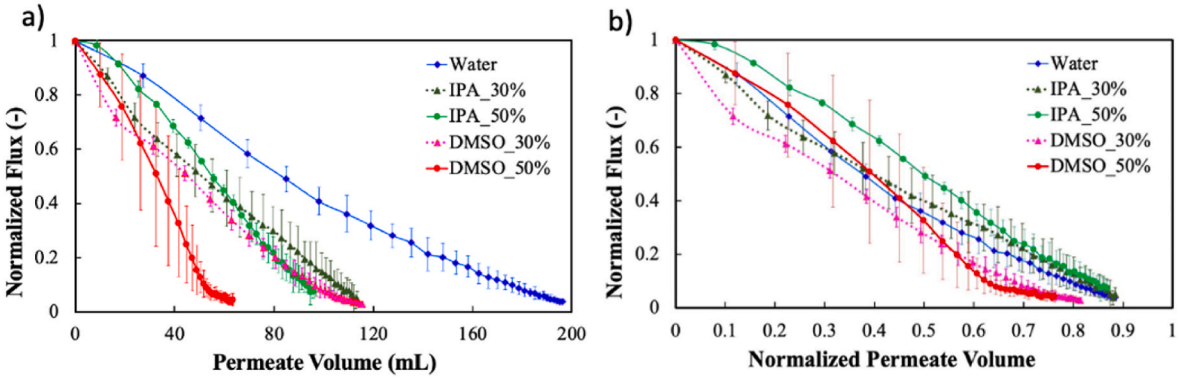

Fig. A1. Trends of normalized flux with respect to (a) accumulated permeate volume and (b) normalized permeate volume (i.e., cumulative permeate volume normalized with respect to the total permeate volume). The feeds were 0.5 g/L lysozyme in different solvent systems and the TMP was constant at 2 bar. Each error bar represents the span of the data obtained from triplicates of each feed.

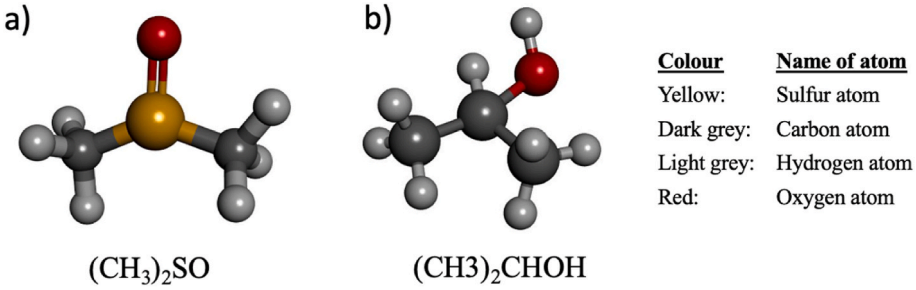

Fig. A2. Chemical structures of (a) dimethyl sulfoxide (DMSO) (b) isopropyl alcohol (IPA) drawn using discovery studio.

Table A1
Properties of molecular structures of DMSO, IPA and water

	DMSO	IPA	Water
van der Waals radius (Å) [68]	6.67	6.55	1.51
Molecular weight (g/mol)	78.1	60.1	18.0
Shape	Tetrahedral	Linear	Bent
Bond angle (°)	109.5	180	104.5
Number of Axis of rotation	3	2	1
Rotational bonds	2	2	0

References

[1] R. van Reis, A. Zydney, Membrane separations in biotechnology, Curr. Opin. Biotechnol. 12 (2) (2001) 208–211, https://doi.org/10.1016/s0958-1669(00)00201-9.
[2] C. Charcosset, Membrane Processes in Biotechnology and Pharmaceutics, Elsevier, 2012.
[3] P.M. Williams, D.L. Oatley-Radcliffe, N. Hilal, Feed solution characterization, in: N. Hilal, A.F. Ismail, T. Matsuura, D. Oatley-Radcliffe (Eds.), Membrane Characterization, Elsevier, 2017, pp. 379–404, https://doi.org/10.1016/b978-0-444-63776-5.00017-6.
[4] H. Li, V. Chen, in: Z.F. Cui, H.S. Muralidhara (Eds.), Membrane Fouling and Cleaning in Food and Bioprocessing, Membrane Technology, Butterworth-Heinemann, Oxford, 2010, pp. 213–254, https://doi.org/10.1016/b978-1-85617-632-3.00010-0.
[5] J.L. Nilsson, Protein fouling of uf membranes: causes and consequences, J. Membr. Sci. 52 (2) (1990) 121–142, https://doi.org/10.1016/s0376-7388(00)80481-0.
[6] A. Matin, T. Laoui, W. Falath, M. Farooque, Fouling control in reverse osmosis for water desalination & reuse: current practices & emerging environment-friendly technologies, Sci. Total Environ. 765 (2021), 142721, https://doi.org/10.1016/j.scitotenv.2020.142721.
[7] J.W. Chew, J. Kilduff, G. Belfort, The behavior of suspensions and macromolecular solutions in crossflow microfiltration: an update, J. Membr. Sci. 601 (2020), 117865, https://doi.org/10.1016/j.memsci.2020.117865.
[8] L. Liu, S. Liu, E. Wang, B. Su, Hollow fiber membrane for organic solvent nanofiltration: a mini review, Membranes 12 (10) (2022) 995, https://doi.org/10.3390/membranes12100995.
[9] H.T. Lay, J.W. Chew, Critical flux of colloidal foulant in microfiltration: effect of organic solvent, J. Membr. Sci. 616 (2020), 118531, https://doi.org/10.1016/j.memsci.2020.118531.
[10] Z. Yin, R.J.E. Yeow, Y. Ma, J.W. Chew, Link between interfacial interaction and membrane fouling during organic solvent ultrafiltration of colloidal foulants, J. Membr. Sci. 611 (2020), 118369, https://doi.org/10.1016/j.memsci.2020.118369.
[11] H.T. Lay, C.S. Ong, R. Wang, J.W. Chew, Choice of DLVO approximation method for quantifying the affinity between latex particles and membranes, J. Membr. Sci. 666 (2023), 121121, https://doi.org/10.1016/j.memsci.2022.121121.
[12] Z. Yin, Y. Ma, B. Tanis-Kanbur, J.W. Chew, Fouling behavior of colloidal particles in organic solvent ultrafiltration, J. Membr. Sci. 599 (2020), 117836, https://doi.org/10.1016/j.memsci.2020.117836.
[13] M.B. Tanis-Kanbur, N.R. Tamilselvam, J.W. Chew, Membrane fouling mechanisms by BSA in aqueous-organic solvent mixtures, J. Ind. Eng. Chem. 108 (2022) 389–399, https://doi.org/10.1016/j.jiec.2022.01.017.
[14] S.K. Zaidi, A. Kumar, Effects of ethanol concentration on flux and gel formation in dead end ultrafiltration of PEG and dextran, J. Membr. Sci. 237 (1) (2004) 189–197, https://doi.org/10.1016/j.memsci.2004.03.017.
[15] R.W. Lencki, S. Williams, Effect of nonaqueous solvents on the flux behavior of ultrafiltration membranes, J. Membr. Sci. 101 (1) (1995) 43–51, https://doi.org/10.1016/0376-7388(94)00282-4.

[16] Q.T. Nguyen, P. Aptel, J. Neel, Characterization of ultrafiltration membranes: Part I. Water and organic-solvent permeabilities, J. Membr. Sci. 5 (1979) 235–251, https://doi.org/10.1016/S0376-7388(00)80451-2.

[17] M.Y. Jaffrin, J.P. Charrier, Optimization of ultrafiltration and diafiltration processes for albumin production, J. Membr. Sci. 97 (1994) 71–81, https://doi.org/10.1016/0376-7388(94)00148-R.

[18] A. Oxley, A.G. Livingston, Anti-fouling membranes for organic solvent nanofiltration (OSN) and organic solvent ultrafiltration (OSU): graft modified polybenzimidazole (PBI), J. Membr. Sci. 662 (2022), 120977, https://doi.org/10.1016/j.memsci.2022.120977.

[19] H. Ebro, Y.M. Kim, J.H. Kim, Molecular dynamics simulations in membrane-based water treatment processes: a systematic overview, J. Membr. Sci. 438 (2013) 112–125.

[20] Y. Ma, J.W. Chew, Investigation of membrane fouling phenomenon using molecular dynamics simulations: a review, J. Membr. Sci. 661 (2022), 120874, https://doi.org/10.1016/j.memsci.2022.120874.

[21] Y. Ma, A.L. Zydney, R. Wang, J.W. Chew, Molecular dynamics study on membrane fouling by oppositely charged proteins, AIChE J. 67 (10) (2021), e17335, https://doi.org/10.1002/aic.17335.

[22] Y. Ma, A.L. Zydney, J.W. Chew, Membrane fouling by lysozyme: effect of local interaction, AIChE J. 67 (7) (2021), e17212.

[23] R.M. Venable, A. Kramer, R.W. Pastor, Molecular dynamics simulations of membrane permeability, Chem. Rev. 119 (9) (2019) 5954–5997, https://doi.org/10.1021/acs.chemrev.8b00486.

[24] A. Mollahosseini, A. Abdelrasoul, Molecular dynamics simulation for membrane separation and porous materials: a current state of art review, J. Mol. Graph. Model. 107 (2021), 107947, https://doi.org/10.1016/j.jmgm.2021.107947.

[25] H.F. Ridgway, J. Orbell, S. Gray, Molecular simulations of polyamide membrane materials used in desalination and water reuse applications: recent developments and future prospects, J. Membr. Sci. 524 (2017) 436–448.

[26] A. Mollahosseini, K. Min Lee, A. Abdelrasoul, H. Doan, N. Zhu, Innovative in situ investigations using synchrotron-based micro tomography and molecular dynamics simulation for fouling assessment in ceramic membranes for dairy and food industry, Int. J. Appl. Ceram. Technol. 18 (6) (2021) 2143–2157, https://doi.org/10.1111/ijac.13824.

[27] Y. Ma, S. Velioğlu, Z. Yin, R. Wang, J.W. Chew, Molecular dynamics investigation of membrane fouling in organic solvents, J. Membr. Sci. 632 (2021), 119329, https://doi.org/10.1016/j.memsci.2021.119329.

[28] I. Jha, A. Rani, P. Venkatesu, Sustained stability and activity of lysozyme in choline chloride against pH induced denaturation, ACS Sustain. Chem. Eng. 5 (9) (2017) 8344–8355.

[29] P. Jolles, J. Jolles, What's new in lysozyme research? Always a model system, today as yesterday, Mol. Cell. Biochem. 63 (2) (1984) 165–189, https://doi.org/10.1007/BF00285225.

[30] Y.-E. Li, Y. Yang, V. Kalthod, S.M. Tyler, Optimization of solvent chasing in API manufacturing process: constant volume distillation, Org. Process Res. Dev. 13 (1) (2008) 73–77, https://doi.org/10.1021/op800152n.

[31] D.E. Pratama, W.C. Hsieh, A. Elmaamoun, H.L. Lee, T. Lee, Recovery of active pharmaceutical ingredients from unused solid dosage-form drugs, ACS Omega 5 (45) (2020) 29147–29157, https://doi.org/10.1021/acsomega.0c03878.

[32] M.C. Cuellar, A.J. Straathof, Downstream of the bioreactor: advancements in recovering fuels and commodity chemicals, Curr. Opin. Biotechnol. 62 (2020) 189–195, https://doi.org/10.1016/j.copbio.2019.11.012.

[33] C.S. Slater, M.J. Savelski, W.A. Carole, D.J. Constable, Solvent use and waste issues, Green chemistry in the pharmaceutical industry (2010) 49–82.

[34] R.M. Parodi, E. Bianchi, A. Ciferri, Thermodynamics of unfolding of lysozyme in aqueous alcohol solutions, J. Biol. Chem. 248 (11) (1973) 4047–4051.

[35] H. Iwase, M. Hirai, S. Arai, S. Mitsuya, S. Shimizu, T. Otomo, M. Furusaka, Comparison of DMSO-induced denaturation of hen egg-white lysozyme and bovine α-lactalbumin, J. Phys. Chem. Solid. 60 (8–9) (1999) 1379–1381.

[36] A.J. Trexler, M.R. Nilsson, The formation of amyloid fibrils from proteins in the lysozyme family, Curr. Protein Pept. Sci. 8 (6) (2007) 537–557, https://doi.org/10.2174/138920307783018659.

[37] N.E. Chayen, E. Saridakis, Is lysozyme really the ideal model protein? J. Cryst. Growth 232 (1–4) (2001) 262–264, https://doi.org/10.1016/s0022-0248(01)01203-9.

[38] S. Jo, T. Kim, V.G. Iyer, W. Im, CHARMM-GUI: a web-based graphical user interface for CHARMM, J. Comput. Chem. 29 (11) (2008) 1859–1865, https://doi.org/10.1002/jcc.20945.

[39] M.B. Tanis-Kanbur, S. Velioğlu, H.J. Tanudjaja, X. Hu, J.W. Chew, Understanding membrane fouling by oil-in-water emulsion via experiments and molecular dynamics simulations, J. Membr. Sci. 566 (2018) 140–150, https://doi.org/10.1016/j.memsci.2018.08.067.

[40] A. Phan, D.R. Cole, A. Striolo, Liquid ethanol simulated on crystalline alpha alumina, J. Phys. Chem. B 117 (14) (2013) 3829–3840, https://doi.org/10.1021/jp312238d.

[41] J. Huang, S. Rauscher, G. Nawrocki, T. Ran, M. Feig, B.L. de Groot, H. Grubmuller, A.D. MacKerell Jr., CHARMM36m: an improved force field for folded and intrinsically disordered proteins, Nat. Methods 14 (1) (2017) 71–73, https://doi.org/10.1038/nmeth.4067.

[42] A.D. MacKerell Jr., M. Feig, C.L. Brooks 3rd, Improved treatment of the protein backbone in empirical force fields, J. Am. Chem. Soc. 126 (3) (2004) 698–699, https://doi.org/10.1021/ja036959e.

[43] S. Plimpton, Fast parallel algorithms for short-range molecular dynamics, J. Comput. Phys. 117 (1) (1995) 1–19.

[44] J.-P. Ryckaert, G. Ciccotti, H.J.C. Berendsen, Numerical integration of the cartesian equations of motion of a system with constraints: molecular dynamics of n-alkanes, J. Comput. Phys. 23 (3) (1977) 327–341, https://doi.org/10.1016/0021-9991(77)90098-5.

[45] M. Wang, J. Wang, J. Jiang, Membrane fouling: microscopic insights into the effects of surface chemistry and roughness, Advanced Theory and Simulations 5 (1) (2021), 2100395, https://doi.org/10.1002/adts.202100395.

[46] S. Tiwari, A. Gogoi, K. Anki Reddy, Effect of an ionic environment on membrane fouling: a molecular dynamics study, Phys. Chem. Chem. Phys. 23 (8) (2021) 5001–5011, https://doi.org/10.1039/d0cp05268j.

[47] W. Humphrey, A. Dalke, K. Schulten, VMD: visual molecular dynamics, J. Mol. Graph. 14 (1) (1996) 27–28, 33-8.

[48] M. Paloncyova, K. Berka, M. Otyepka, Convergence of free energy profile of coumarin in lipid bilayer, J. Chem. Theor. Comput. 8 (4) (2012) 1200–1211, https://doi.org/10.1021/ct2009208.

[49] D.J. Evans, B.L. Holian, The nose–hoover thermostat, J. Chem. Phys. 83 (8) (1985) 4069–4074, https://doi.org/10.1063/1.449071.

[50] Q. Wei, W. Zhao, Y. Yang, B. Cui, Z. Xu, X. Yang, Method evaluations for adsorption free energy calculations at the solid/water interface through metadynamics, umbrella sampling, and jarzynski's equality, ChemPhysChem 19 (6) (2018) 690–702, https://doi.org/10.1002/cphc.201701241.

[51] E.G. Brandt, A.P. Lyubartsev, Molecular dynamics simulations of adsorption of amino acid side chain analogues and a titanium binding peptide on the TiO2 (100) surface, J. Phys. Chem. C 119 (32) (2015) 18126–18139, https://doi.org/10.1021/acs.jpcc.5b02670.

[52] Y. Xiang, R.G. Xu, Y. Leng, Molecular dynamics simulations of a poly(ethylene glycol)-grafted polyamide membrane and its interaction with a calcium alginate gel, Langmuir 32 (18) (2016) 4424–4433, https://doi.org/10.1021/acs.langmuir.6b00348.

[53] Z. Zhang, T. Wu, Q. Wang, H. Pan, R. Tang, Impact of interfacial high-density water layer on accurate estimation of adsorption free energy by Jarzynski's equality, J. Chem. Phys. 140 (3) (2014), 034706, https://doi.org/10.1063/1.4858428.

[54] S.W. Hung, P.Y. Hsiao, C.C. Chieng, Dynamic information for cardiotoxin protein desorption from a methyl-terminated self-assembled monolayer using steered molecular dynamics simulation, J. Chem. Phys. 134 (19) (2011), 194705, https://doi.org/10.1063/1.3592559.

[55] S. Lecot, Y. Chevolot, M. Phaner-Goutorbe, C. Yeromonahos, Impact of silane monolayers on the adsorption of streptavidin on silica and its subsequent interactions with biotin: molecular dynamics and steered molecular dynamics simulations, J. Phys. Chem. B 124 (31) (2020) 6786–6796, https://doi.org/10.1021/acs.jpcb.0c04382.

[56] T. Utesch, G. Daminelli, M.A. Mroginski, Molecular dynamics simulations of the adsorption of bone morphogenetic protein-2 on surfaces with medical relevance, Langmuir 27 (21) (2011) 13144–13153, https://doi.org/10.1021/la202489w.

[57] S. Park, F. Khalili-Araghi, E. Tajkhorshid, K. Schulten, Free energy calculation from steered molecular dynamics simulations using Jarzynski's equality, J. Chem. Phys. 119 (6) (2003) 3559–3566, https://doi.org/10.1063/1.1590311.

[58] R.H. Meissner, G. Wei, L.C. Ciacchi, Estimation of the free energy of adsorption of a polypeptide on amorphous SiO2 from molecular dynamics simulations and force spectroscopy experiments, Soft Matter 11 (31) (2015) 6254–6265, https://doi.org/10.1039/c5sm01444a.

[59] A.D. Marshall, P.A. Munro, G. Trägårdh, The effect of protein fouling in microfiltration and ultrafiltration on permeate flux, protein retention and selectivity: a literature review, Desalination 91 (1) (1993) 65–108, https://doi.org/10.1016/0011-9164(93)80047-q.

[60] H.J. Tanudjaja, A. Anantharaman, A.Q.Q. Ng, Y. Ma, M.B. Tanis-Kanbur, A. L. Zydney, J.W. Chew, A review of membrane fouling by proteins in ultrafiltration and microfiltration, J. Water Process Eng. 50 (2022), 103294, https://doi.org/10.1016/j.jwpe.2022.103294.

[61] J. Chen, M. Zhang, F. Li, L. Qian, H. Lin, L. Yang, X. Wu, X. Zhou, Y. He, B.Q. Liao, Membrane fouling in a membrane bioreactor: high filtration resistance of gel layer and its underlying mechanism, Water Res. 102 (2016) 82–89, https://doi.org/10.1016/j.watres.2016.06.028.

[62] G. Fiorin, M.L. Klein, J. Hénin, Using collective variables to drive molecular dynamics simulations, Mol. Phys. 111 (22–23) (2013) 3345–3362, https://doi.org/10.1080/00268976.2013.813594.

[63] J.A. Willemsen, S.C. Myneni, I.C. Bourg, Molecular dynamics simulations of the adsorption of phthalate esters on smectite clay surfaces, J. Phys. Chem. C 123 (22) (2019) 13624–13636.

[64] C. Bartels, Analyzing biased Monte Carlo and molecular dynamics simulations, Chem. Phys. Lett. 331 (5–6) (2000) 446–454, https://doi.org/10.1016/s0009-2614(00)01215-x.

[65] Equilibrium properties of simple fluids, in: D.C. Rapaport (Ed.), The Art of Molecular Dynamics Simulation, Cambridge University Press, Cambridge, 2004, pp. 83–119, https://doi.org/10.1017/cbo9780511816581.007.

[66] R. Zhang, W. Yan, C. Jing, Experimental and molecular dynamic simulation study of perfluorooctane sulfonate adsorption on soil and sediment components, J. Environ. Sci. (China) 29 (2015) 131–138, https://doi.org/10.1016/j.jes.2014.11.001.

[67] T. Wei, M.A. Carignano, I. Szleifer, Lysozyme adsorption on polyethylene surfaces: why are long simulations needed? Langmuir 27 (19) (2011) 12074–12081, https://doi.org/10.1021/la202622s.

[68] S.S. Batsanov, Van der Waals radii of elements, Inorg. Mater. 37 (9) (2001) 871–885.